Published in final edited form as:
Magn Reson Med. 2009 April ; 61(4): 970–974. doi:10.1002/mrm.21928.

Feasibility of Concurrent Dual Contrast Enhancement Using CEST Contrast Agents and Superparamagnetic Iron Oxide Particles

Assaf A. Gilad[1,2], **Hanneke W.M. van Laarhoven**[1,2,3], **Michael T. McMahon**[1,4], **Piotr Walczak**[1,2], **Arend Heerschap**[5], **Michal Neeman**[6], **Peter C.M. van Zijl**[1,4], and **Jeff W.M. Bulte**[1,2,7,8]

[1] Russell H. Morgan Department of Radiology and Radiological Science, Division of MR Research, Neurosection, Johns Hopkins University School of Medicine, Baltimore, Maryland, USA [2] Cellular Imaging Section and Vascular Biology Program, Institute for Cell Engineering, Johns Hopkins University School of Medicine, Baltimore, Maryland, USA [3] Department of Medical Oncology, Radboud University Nijmegen Medical Centre, Nijmegen, the Netherlands [4] F. M. Kirby Research Center for Functional Brain Imaging, Kennedy Krieger Institute, Baltimore, Maryland, USA [5] Department of Radiology, Radboud University Nijmegen Medical Centre, Nijmegen, the Netherlands [6] Department of Biological Regulation, The Weizmann Institute of Science, Rehovot, Israel [7] Department of Chemical and Biomolecular Engineering, Whiting School of Engineering, Johns Hopkins University [8] Department of Biomedical Engineering, Whiting School of Engineering, Johns Hopkins University

Abstract

A major challenge for cellular and molecular MRI is to study interactions between two different cell populations or biological processes. We studied the possibility to simultaneously image contrast agents based on two different MRI contrast mechanisms: chemical exchange saturation transfer (CEST) and enhancement of T2 relaxation. Various amounts of superparamagnetic iron oxide (SPIO) nanoparticles were mixed with a fixed concentration (250 μM) of the CEST agent poly-L-lysine. T2 maps, CEST maps, and frequency-dependent saturation spectra were then measured. Color-coded overlay maps demonstrated the feasibility of concurrent dual contrast enhancement. We found that at concentrations lower than 5 μg(Fe)/ml both contrast agents can be imaged simultaneously. At higher concentrations the iron-based agent can be used to "shut off" the signal arising from the CEST agent. These initial findings are a first step towards using dual CEST/T2 contrast imaging for studying multiple cellular or molecular targets simultaneously *in vivo*.

Keywords

CEST agent; superparamagnetic iron oxide; molecular imaging

Corresponding author: Assaf A. Gilad, The Johns Hopkins University School of Medicine, Russell H. Morgan Department of Radiology and Radiological Science, Division of MR Research, 1550 Orleans St. Cancer Research Building II, Room 4M63, Baltimore, MD 21231, Phone 410-502-8188, assaf@mri.jhu.edu.

Introduction

Recently, a new type of MRI contrast has been developed that relies on selective labeling of protons on contrast agents using a radiofrequency (RF) saturation pulse followed by transfer of saturation via exchange to bulk water, producing a fractional reduction in the water signal. As a result, these agents are being referred to as chemical exchange saturation transfer (CEST) contrast agents (1). A variety of organic (1–4) and organometallic (5–8) compounds have a sufficient number of protons to be detected at low concentrations and with suitable chemical exchange rates and chemical shifts to be selectively labeled.

CEST contrast agents have a major advantage in that they are switchable, i.e., the contrast is detectable only when a saturation pulse is applied at the specific frequency where the agent's exchangeable protons resonate. Recently, its application has been demonstrated for imaging of cells using an artificial lysine-rich protein (LRP) as CEST agent (9). The switchable "on-off" property raises the possibility for CEST agents to coexist with T1 and T2 contrast agents, potentially enabling simultaneously imaging and tracking of two different targets such as two cell populations at the same location. Before such studies are undertaken, however, the interactions between these two different contrast mechanisms should be examined carefully.

Among the previously reported diamagnetic CEST contrast agents, Poly-L-Lysine (PLL) has a high exchange rate as well as multiple exchangeable protons resulting in amplification of contrast by several orders of magnitude (3). Our initial CEST reporter gene is designed based on these properties of PLL (9) and can produce a relatively constant intracellular concentration in cells independent of cell division. A different source of cellular contrast (T2) may be obtained by using superparamagnetic agents, either by labeling with iron oxide (SPIO) particles (10) or by overexpression of ferritin as an MRI reporter gene (11–13). In order to assess the feasibility of using CEST and iron oxide-induced contrast simultaneously, we conducted an *in vitro* study using both agents. The results show a range of concentrations in which the two contrast agents can be used concurrently and distinguished from each other.

Materials and Methods

A phantom composed of glass NMR tube, 5 mm in diameter, containing 5 inner capillaries tubes, each with or without 250μM PLL, (MW 22 kDa, Sigma St. Louis, MO, USA) and different concentrations of SPIO (Feridex, 0–50 μg Fe/ml) were imaged at 11.7 T using a Bruker MR spectrometer (using the software Paravision 3.0.2). For T2 measurements, a spin-echo sequence was used (TR=3000 ms, TE=9.2, 20, 30, 40, 50, 60, 70, 80 and, 90 ms), with a single scan being acquired for each echo time. CEST imaging was performed with the parameters TR/TE=9000/6.35 ms, saturation power=0.5μT, saturation time=4000 ms, and Δω=± 3.76 ppm from the water ^{1}H frequency (to coincide with the PLL amide protons at +3.76 ppm and for a control measurement at −3.76 ppm). A single 1 mm slice was acquired with a field of view 5×5 mm and a matrix size of 32×32 pixels with an in plane resolution of 156 μm. The total voxel volume was 2.43×10^{-5} ml.

MR data were analyzed using MATLAB 5.6.1 (MathWorks). Maps of change in signal intensity (MTR_{asym}) were generated pixel by pixel from $[[S_w{}^{-\Delta\omega} - S_w{}^{+\Delta\omega}]/S_w{}^{-\Delta\omega}]\times100$, where $S_w{}^{-\Delta\omega}$ and $S_w{}^{+\Delta\omega}$ are the average water signal intensities of 4 images acquired with a saturation at Δω=±3.76 ppm from the water ^{1}H frequency. T2 was determined from 1/R2 derived using a linear regression of log (MR signal) as function of TE.

Theory

When using a spin echo imaging sequence with echo time, TE, the signal S without applying a saturation pulse can be given by the following expression:

$$S = S_0(1 - e^{-TR \bullet R_1})e^{-TE \bullet R_2} \quad [1]$$

In this, the relaxation rates are given by

$$R_i = R_{i0} + [Fe] * R_i^{conc} \quad [2]$$

In which i=1,2 and R_i^{conc} is the relaxivity.

CEST contrast is generally observed using the signal difference between two images, one with the saturation pulse on resonance with the exchangeable peak, $S_w^{+\Delta\omega}$, and the second with the saturation pulse on the opposite side of water, $S_w^{-\Delta\varpi}$, with water being assigned to 0 ppm. The difference contrast or magnetization transfer ratio asymmetry (MTR_{asym}) is then:

$$MTR_{asym} = \frac{S_w^{-\Delta\omega} - S_w^{+\Delta\omega}}{S_w^{-\Delta\omega}} \quad [3]$$

This expression is commonly related to the proton transfer ratio (PTR):

$$MTR_{asym} \approx PTR = \frac{S_{0w} - S_w^{+\Delta\omega}(t_{sat}\alpha)}{S_{0w}} = \frac{k_{sw} \bullet \alpha \bullet x_{CA}}{R_{1w} + k_{sw} \bullet x_{CA}} \times [1 - e^{-(R_{1w} + k_{sw} \bullet x_{CA})t_{sat}}] \quad [4]$$

in which S_{0w} is the signal without saturation and ksw is the contrast agent (solute)-water exchange rate, x_{CA} is the fractional concentration of exchangeable protons of the contrast agent, t_{sat} is the saturation time, α is the saturation efficiency, and the term $k_{sw}x_{CA}$ accounts for back exchange of saturated water protons to the contrast agent, which will occur when the exchange rates and/or the concentration of exchangeable protons for the CEST agent are very high. This asymmetry analysis with respect to water partially corrects for direct saturation effects that contribute to saturation and is not included in the PTR expression. When studying the interaction between these two contrast agent types, direct saturation becomes more important because the presence of a T2* agent will increase the direct saturation contribution at the CEST agent frequency through broadening the water line. The saturation factor α is determined as:

$$\alpha = \omega_1^2 / \omega_1^2 + pq \quad [5]$$

in which

$$p = R_{2s} + k_{sw} - k_{sw}^2 \bullet X_{CA} / (R_{2w} + k_{sw} \bullet X_{CA}) \quad [6]$$

$$q = R_{1s} + k_{sw} - k_{sw}^2 \bullet X_{CA} / (R_{1w} + k_{sw} \bullet X_{CA}) \quad [7]$$

Thus, R_1 and R_2 contrast agents can affect the CEST effect through p and q.

Results

An MRI phantom was used in order to study the interactions between SPIO and CEST contrast agents. Figure 1 shows a proton density image of the phantom and the corresponding CEST and T2 maps. The change in signal intensity as a function of iron concentration is summarized in Table 1. In the presence of 250 μM PLL and iron oxide concentrations up to 0.5 μg Fe/ml, the MTR_{asym} was found to be around 12%. One side remark is that all samples contained PLL without iron oxide were placed in capillaries with a thinner diameter which might led to susceptibility effects and lower MTR_{asym}. At higher iron concentrations (5 μg Fe/ml and above) the CEST contrast starts to drop. The frequency dependent saturation spectrum (called Z-spectrum or CEST spectrum) in Fig. 2 demonstrates that higher Fe concentrations induce line broadening, which resulted in a disappearance of the hallmark CEST “dip” in water intensity at the amide proton frequency. The drop in CEST effect at high iron concentration is due to an increase in direct water saturation at the exchangeable proton frequency.

As expected, the reduction in T2 shows a linear dependence (R^2=0.92) on the iron concentration indicating that this process is independent of the concurrent presence of PLL. This finding is further supported by comparing the T2 values of two samples containing 0.5 μg(Fe)/ml with and without PLL (Table 1), where no significant difference was observed between the two samples (unpaired 2-tailed t-Test, p=0.87).

A merged image of the R2 map and CEST map is shown in Fig. 3. From these results, it is evident that the iron- and CEST-induced contrast can be distinguished from each other under concurrent conditions.

Discussion

Combining CEST-labeling and SPIO-labeling may have potential applications in serial studies that require simultaneous imaging of two cell populations. In the scenario of different locations of cell injections, differential migration patterns may be visualized. In addition, two cell populations may be identified separately when injected at the same location but at two different time points. One such example is studying stem cell-tumor cell interactions. Neural stem cells can exhibit extensive migration directed by trophic factors secreted by glioma cells, offering new opportunities for drug delivery or homing of cells expressing anti-tumor genes (14,15). Another example exists for interactions between mesenchymal stem cells and certain immune cells (16). Techniques that allow labeling and imaging of two cell types simultaneously may aid in optimizing cell therapies based on tumor cell/stem cell interactions. As a first step, the present study has investigated the co-existence of CEST and T2 contrast mechanisms and indicates a range of contrast agent concentrations where such a dual labeling approach may be feasible.

In the phantom containing PLL and 0.5 μg Fe/ml, each voxel contains 12 pg of iron, which is comparable to 1–2 labeled cells per voxel (17). It was found that this concentration does not affect the CEST contrast. For a higher concentration of 5 μg Fe/ml, a reduction in the CEST effect is observed from 11.9% to 10.3%. When extrapolated, this is proportional to about 10–20 labeled cells. At 50 μg Fe/ml (proportional to 100–200 cells), an almost

complete abolition of the CEST contrast was observed. Thus, assuming a total of about 20–200 $\times 10^3$ cells per voxel, if only 0.5% to 0.05% of the cells in a voxel are labeled (equal to 50 μg Fe/ml), there will be total elimination of the CEST contrast for this particular amide proton based agent. Based on the *in vitro* measurements, our findings suggest that there is a range of concentrations of PLL and iron oxide in which both contrast mechanisms can co-exist. Nevertheless, a high number of SPIO-labeled cells may eliminate all CEST contrast. Thus, regions rich in iron (such as liver or spleen) or tissues containing large number of SPIO-labeled cells may potentially preclude the use of CEST agents. Recent studies have used a similar principle of off-resonance saturation to detect the presence of SPIO in phantoms (18) or iron deposits present in the brain (19). In both cases an off-resonance saturation pulse was applied prior to signal acquisition. Since iron broadens the water line the contrast will be increased as a result of direct saturation. However, if used properly, the changes in CEST contrast can be used as a sensor for the presence of SPIO particles and SPIO-labeled cells. When SPIO-labeled cells are migrating, the arrival and accumulation at the site containing CEST contrast (i.e. tissue containing LRP-labeled cells (9)) could be verified by a reduction in the MTR_{asym}. This approach can be considered to be analogous to the Fluorescent Resonant Energy Transfer (FRET) imaging capabilities of fluorescent reporter genes (20).

Another approach for multiple labeling of different cells for MRI relies purely on CEST agents. Two PARACEST agents with different chemical shift values were used for labeling of two cell populations and their distinction using MRI (21). A recent study by the same group showed that manipulating the shape of liposomes containing PARACEST agents can create differences in the chemical shift which, in turn, can be useful for differential labeling of multiple targets (22). We have recently showed that certain polypeptides with different exchangeable protons are distinguishable one from another *in vitro* with potential for multiple labeling studies (23). MRI detection of two cell populations has been demonstrated *in vivo* by labeling one cell population with SPIO as a T2 agent and the other one with manganese oxide nanoparticles as a T1 agent. Both cell populations were detected and could be distinguished from another within the same imaging plane (24).

In this study we have used high PLL:SPIO ratios in order to minimize the effect of direct binding of the iron oxide particles to the PLL, which by itself may alter contrast through the formation of larger complexes. It is known that aggregation of SPIO through (biological) complexation shortens the T2 as compared to an equivalent concentration of uncomplexed nanoparticles (25). Furthermore, it is important to keep in mind that, *in vivo*, the CEST contrast agent concentration may be below the 12% baseline value of this study. It should, however, be possible to detect CEST effects of one percent or higher, i.e. similar to the magnitude of typical fMRI signal changes, by comparing the signal intensity with and without saturation and the asymmetry of the saturation using statistical approaches.

Acknowledgments

Supported by NIH grants R21 EB005252 (JWMB), and K01 EB006394 (MTM).

References

1. Ward KM, Aletras AH, Balaban RS. A new class of contrast agents for MRI based on proton chemical exchange dependent saturation transfer (CEST). J Magn Reson. 2000; 143(1):79–87. [PubMed: 10698648]
2. Ward KM, Balaban RS. Determination of pH using water protons and chemical exchange dependent saturation transfer (CEST). Magn Reson Med. 2000; 44(5):799–802. [PubMed: 11064415]

3. McMahon MT, Gilad AA, Zhou J, Sun PZ, Bulte JW, van Zijl PC. Quantifying exchange rates in chemical exchange saturation transfer agents using the saturation time and saturation power dependencies of the magnetization transfer effect on the magnetic resonance imaging signal (QUEST and QUESP): Ph calibration for poly-L-lysine and a starburst dendrimer. Magn Reson Med. 2006; 55(4):836–847. [PubMed: 16506187]
4. van Zijl PC, Jones CK, Ren J, Malloy CR, Sherry AD. MRI detection of glycogen in vivo by using chemical exchange saturation transfer imaging (glycoCEST). Proc Natl Acad Sci U S A. 2007; 104(11):4359–4364. [PubMed: 17360529]
5. Aime S, Barge A, Delli Castelli D, Fedeli F, Mortillaro A, Nielsen FU, Terreno E. Paramagnetic lanthanide(III) complexes as pH-sensitive chemical exchange saturation transfer (CEST) contrast agents for MRI applications. Magn Reson Med. 2002; 47(4):639–648. [PubMed: 11948724]
6. Zhang S, Merritt M, Woessner DE, Lenkinski RE, Sherry AD. PARACEST agents: modulating MRI contrast via water proton exchange. Acc Chem Res. 2003; 36(10):783–790. [PubMed: 14567712]
7. Vinogradov E, He H, Lubag A, Balschi JA, Sherry AD, Lenkinski RE. MRI detection of paramagnetic chemical exchange effects in mice kidneys in vivo. Magn Reson Med. 2007; 58(4): 650–655. [PubMed: 17899603]
8. Yoo B, Pagel MD. A PARACEST MRI contrast agent to detect enzyme activity. J Am Chem Soc. 2006; 128(43):14032–14033. [PubMed: 17061878]
9. Gilad AA, McMahon MT, Walczak P, Winnard PT Jr, Raman V, van Laarhoven HW, Skoglund CM, Bulte JW, van Zijl PC. Artificial reporter gene providing MRI contrast based on proton exchange. Nat Biotechnol. 2007; 25(2):217–219. [PubMed: 17259977]
10. Bulte JW, Kraitchman DL. Iron oxide MR contrast agents for molecular and cellular imaging. NMR in biomedicine. 2004; 17(7):484–499. [PubMed: 15526347]
11. Genove G, Demarco U, Xu H, Goins WF, Ahrens ET. A new transgene reporter for in vivo magnetic resonance imaging. Nat Med. 2005:450–454. [PubMed: 15778721]
12. Cohen B, Dafni H, Meir G, Harmelin A, Neeman M. Ferritin as an endogenous MRI reporter for noninvasive imaging of gene expression in C6 glioma tumors. Neoplasia. 2005; 7(2):109–117. [PubMed: 15802016]
13. Cohen B, Ziv K, Plaks V, Israely T, Kalchenko V, Harmelin A, Benjamin LE, Neeman M. MRI detection of transcriptional regulation of gene expression in transgenic mice. Nat Med. 2007; 13(4):498–503. [PubMed: 17351627]
14. Barresi V, Belluardo N, Sipione S, Mudo G, Cattaneo E, Condorelli DF. Transplantation of prodrug-converting neural progenitor cells for brain tumor therapy. Cancer Gene Ther. 2003; 10(5):396–402. [PubMed: 12719709]
15. Tang Y, Shah K, Messerli SM, Snyder E, Breakefield X, Weissleder R. In vivo tracking of neural progenitor cell migration to glioblastomas. Hum Gene Ther. 2003; 14(13):1247–1254. [PubMed: 12952596]
16. Chen X, Armstrong MA, Li G. Mesenchymal stem cells in immunoregulation. Immunol Cell Biol. 2006; 84(5):413–421. [PubMed: 16869941]
17. Walczak P, Kedziorek DA, Gilad AA, Lin S, Bulte JW. Instant MR labeling of stem cells using magnetoelectroporation. Magn Reson Med. 2005; 54(4):769–774. [PubMed: 16161115]
18. Zurkiya O, Hu X. Off-resonance saturation as a means of generating contrast with superparamagnetic nanoparticles. Magn Reson Med. 2006; 56(4):726–732. [PubMed: 16941618]
19. Smith, SA.; Bulte, JWM.; van Zijl, PCM. Using Direct Water Saturation for Sensitive Detection of Iron in the Human Brain. Proceedings of the Joint Annual Meeting ISMRM-ESMRMB; Germany, Berlin. 2007. p. 2168
20. Jares-Erijman EA, Jovin TM. FRET imaging. Nat Biotechnol. 2003; 21(11):1387–1395. [PubMed: 14595367]
21. Aime S, Carrera C, Delli Castelli D, Geninatti Crich S, Terreno E. Tunable imaging of cells labeled with MRI-PARACEST agents. Angewandte Chemie (International ed. 2005; 44(12):1813–1815.

22. Terreno E, Castelli DD, Milone L, Rollet S, Stancanello J, Violante E, Aime S. First ex-vivo MRI co-localization of two LIPOCEST agents. Contrast Media Mol Imaging. 2008; 3(1):38–43. [PubMed: 18335476]

23. McMahon MT, Gilad AA, DeLiso MA, Cromer Berman SM, Bulte JWM, van Zijl PCM. New "Multi-Color" Polypeptide DIACEST Contrast Agents for MR Imaging. Magn Reson Med. 2008; 60(3):803–812. [PubMed: 18816830]

24. Gilad AA, Walczak P, McMahon MT, Na HB, Lee JH, An K, Hyeon T, van Zijl PC, Bulte JW. MR tracking of transplanted cells with "positive contrast" using manganese oxide nanoparticles. Magn Reson Med. 2008; 60(1):1–7. [PubMed: 18581402]

25. Perez JM, Josephson L, O'Loughlin T, Hogemann D, Weissleder R. Magnetic relaxation switches capable of sensing molecular interactions. Nat Biotechnol. 2002; 20(8):816–820. [PubMed: 12134166]

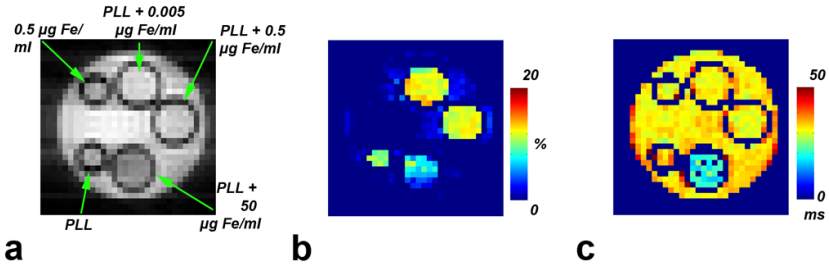

Figure 1. Phantom layout with the corresponding CEST and T2 maps

a) Proton density image of capillaries containing different iron concentrations (0–50 μg (Fe)/ml) with or without the presence of 250 μM PLL. b) CEST map showing the MTR_{asym} calculated as the percent of signal change between RF irradiation at $\Delta\omega=\pm 3.76$ppm. c) T2 map acquired for the same phantom. The figure is representative of three independent experiments.

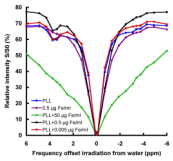

Figure 2. Saturation spectra

mean relative signal intensities of the samples as a function of saturation frequency. The reduction in the signal intensity at $\Delta\omega$=3.76ppm from the water ^{1}H frequency at 0 ppm is a specific CEST effect due to amide proton exchange in PLL. The increase in Fe concentration broadens the water line and explains the elimination of this CEST effect at higher iron concentrations.

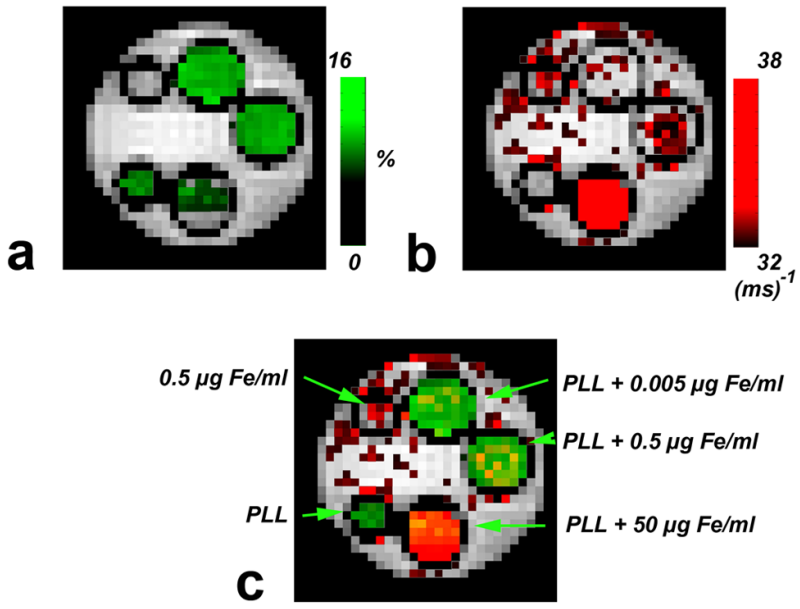

Figure 3. Concurrent dual MRI contrast

a) CEST **(**MTR_{asym}**)** map. b) R2 (1/T2) map of the same phantom. c) overlay of the maps a and b. The color-coded map shows that PLL and iron oxides can be distinguished from each other at lower concentrations, at higher concentrations the SPIO can “switch off” the CEST contrast.

Table 1

			MTR_{asym} (%)[1]		T2 (ms)[2]	
Fe(μg/ml)	**PLL**	**N[3]**	**Average[4]**	**S.D**	**Average**	**S.D**
0	250 μM	3	10.1	2.6	35.6	2.7
0.005	250 μM	1	12.1	N/A	31.0	N/A
0.05	250 μM	2	12.7	1.9	33.0	2.1
0.5	250 μM	3	11.9	1.2	31.9	3.5
0.5	0	3	0.1	0.5	32.6	5.9
5	250 μM	2	10.3	0.2	28.1	5.4
50	250 μM	1	1.0	N/A	16.0	N/A

[1] MTR_{asym} was derived from the mean change in signal intensity in the CEST maps $[[S_W{}^{-\Delta\omega} - S_W{}^{+\Delta\omega}]/S_W{}^{-\Delta\omega}]\times 100$.

[2] T2 was derived from the mean of region of interest form the T2 maps.

[3] N is the number of independent experiments for each capillary.

[4] The average is of the independent experiments (N).